iScience

CellPress

Article

Interfacial Effects on the Band Edges of Ta_3N_5 Photoanodes in an Aqueous Environment: A Theoretical View

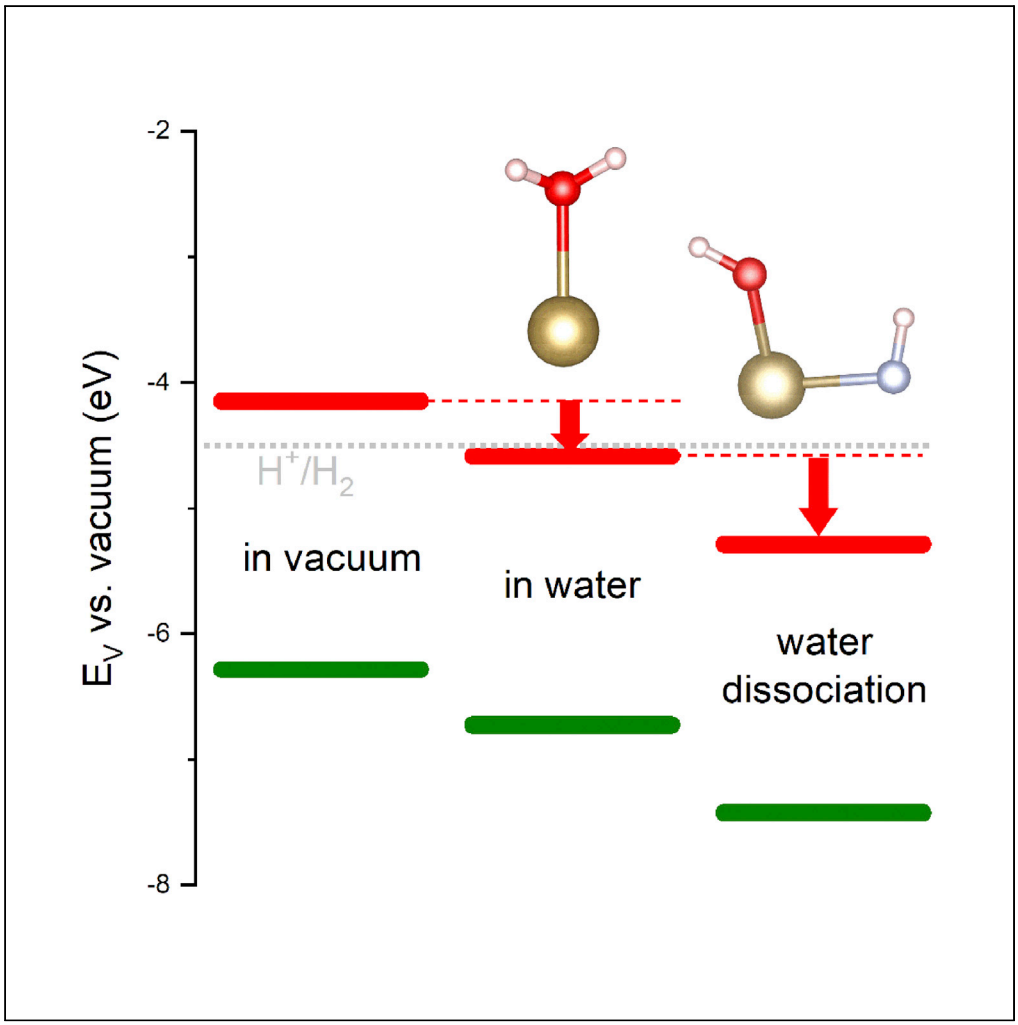

Guozheng Fan, Tao Fang, Xin Wang, ..., Jianyong Feng, Zhaosheng Li, Zhigang Zou

zsli@nju.edu.cn

HIGHLIGHTS

We have studied interfacial effects on the band edges of Ta_3N_5 in an aqueous environment

Both water and the hydroxylated surface promote the formation of the interface dipole

High onset potentials of Ta_3N_5 may be ascribed to negative shift of band edge potentials

Fan et al., iScience *13*, 432–439
March 29, 2019
https://doi.org/10.1016/j.isci.2019.02.024

iScience

CellPress

Article

Interfacial Effects on the Band Edges of Ta_3N_5 Photoanodes in an Aqueous Environment: A Theoretical View

Guozheng Fan,[1] Tao Fang,[1] Xin Wang,[1] Yaodong Zhu,[1] Hongwei Fu,[1] Jianyong Feng,[1] Zhaosheng Li,[1,2,3,*] and Zhigang Zou[1,2]

SUMMARY

Ta_3N_5, as a fascinating photoanode for solar hydrogen production, is expected to split water without any bias, because its band edge potentials straddle H_2O redox potentials. Unfortunately, Ta_3N_5 photoanodes can split water only when a bias of at least 0.6–0.9 V is applied. It means that they exhibit an onset potential as high as 0.6–0.9 V_{RHE} (reversible hydrogen electrode). In this study, density functional theory calculations show that the band edge potentials of Ta_3N_5 have a shift of approximately −0.42 eV relative to vacuum level when exposed to water. The increased ratio of dissociated water at Ta_3N_5-water interface will further make the band edge potentials shift −0.85 eV relative to vacuum level, implying the anodic shifts of the onset potential for water oxidation. The findings may reveal the mystery of the unexpectedly high onset potential of Ta_3N_5, as high as 0.6–0.9 V_{RHE}.

INTRODUCTION

Because the available solar energy is inexhaustible and pollution-free, energy harvested directly from sunlight is a prospective way to solve the problems arising from fossil fuel consumption. Among all the utilization of solar energy conversion and storage, photoelectrochemical (PEC) water splitting, which mimics natural photosynthesis, is very attractive, because PEC-based tandem cells for water splitting exhibit theoretical solar-to-hydrogen efficiency of 29.7% (Hu et al., 2013; Chen et al., 2018). In general, suitable band gaps and band edge potentials are the primary condition when designing the PEC tandem cell system for solar water splitting. Ta_3N_5 with band gap of 2.1 eV is a promising photoanode candidate for overall water splitting (Higashi et al., 2011; Li et al., 2013a, 2013b, 2015). As its band edge potentials straddle H_2O redox potentials, it is possible to split water with very small bias or even without any bias (Chun et al., 2003; Wang et al., 2014; Fan et al., 2017). In other words, its onset potential for water oxidation may be close to 0 V_{RHE} (reversible hydrogen electrode) (Chun et al., 2003; Wang et al., 2014; Fan et al., 2017).

Although near-theoretical-limit photocurrent densities for water oxidation on Ta_3N_5 have already been reported (Liu et al., 2016), a large bias of at least 0.6–0.9 V is required for water splitting over a single Ta_3N_5 photoanode in the experiments (Liu et al., 2016; Li et al., 2013a, 2013b; Seo et al., 2015; Wang et al., 2016; Zhang et al., 2016; Zhong et al., 2017; Chen et al., 2013). The solar-to-hydrogen efficiency of Ta_3N_5 photoanodes are greatly being hindered by unexpectedly high onset potentials (0.6–0.9 V_{RHE}) (Liu et al., 2016; Li et al., 2013a, 2013b; Seo et al., 2015; Wang et al., 2016; Zhang et al., 2016; Zhong et al., 2017; Chen et al., 2013). This problem has been plaguing chemists and materials scientists for many years. Therefore, it is of great significance to understand what causes the high onset potentials of Ta_3N_5 photoanodes.

Oxygen defects in the bulk are easy to be introduced during the synthesis process of Ta_3N_5 photoanodes. In our previous study, density functional theory (DFT) calculations have revealed that these oxygen impurities in the bulk Ta_3N_5 make its band edge potentials relative to vacuum shift approximately −0.2 eV (Fan et al., 2017; Wang et al., 2015a, 2015b). The influence of these oxygen defects in the bulk only partially helps to explain the high onset potential for water oxidation (van de Krol and Grätzel, 2012; Selcuk and Selloni, 2016; Bard and Fox, 1995). However, it cannot interpret why the onset potentials for water oxidation are as high as 0.6–0.9 V_{RHE} even when oxygen evolution reaction (OER) electrocatalysts are loaded on the surface of Ta_3N_5 photoanodes.

Very recently, catalyst-water interfaces have been found to significantly affect the electronic structures and catalytic performances (He et al., 2016; Onda et al., 2005; Pham et al., 2014, 2017; Kharche et al., 2014; Hu

[1]Collaborative Innovation Center of Advanced Microstructures, National Laboratory of Solid State Microstructures, College of Engineering and Applied Sciences, Nanjing University, Nanjing 210093, P. R. China

[2]Jiangsu Key Laboratory for Nano Technology, Nanjing University, Nanjing 210093, P. R. China

[3]Lead Contact

*Correspondence: zsli@nju.edu.cn

https://doi.org/10.1016/j.isci.2019.02.024

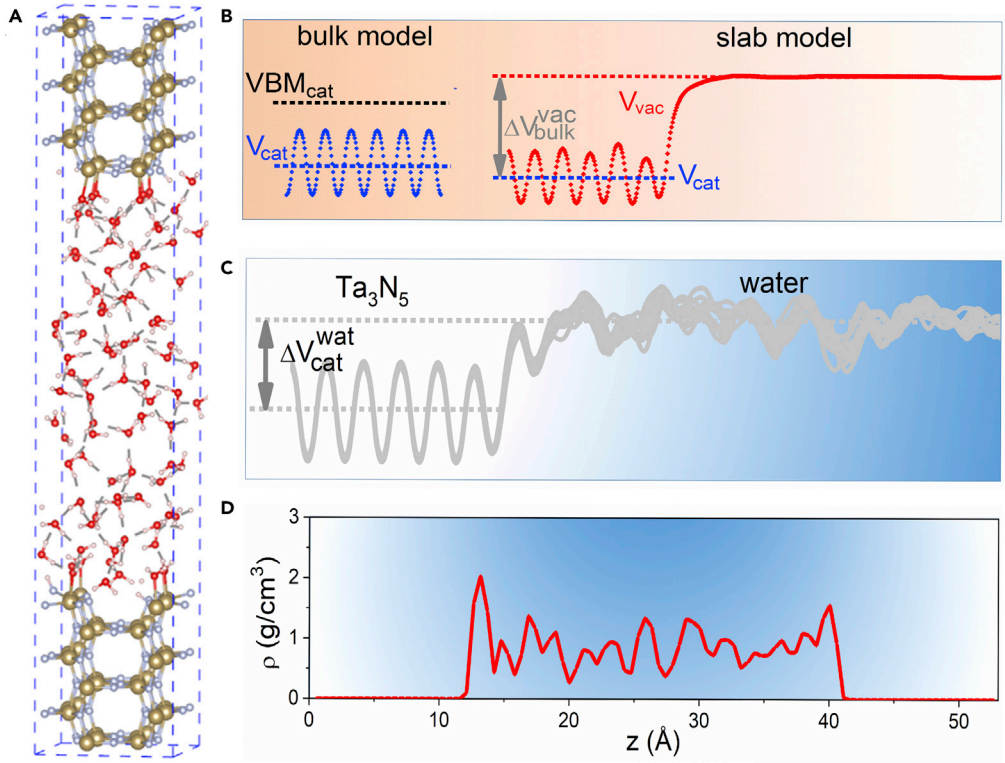

Figure 1. Ta_3N_5-Water Interfaces

(A) Atomic structure of the snapshot of equilibrated Ta_3N_5-water unit cell. The clay brown, light blue, red, and light pink balls represent Ta, N, O, and H atoms, respectively.

(B) Simplified schematic diagram of the band edge potentials of Ta_3N_5 relative to vacuum. VBM_{cat}, V_{cat}, V_{vac}, and ΔV_{bulk}^{vac} are the energy level of the VBM of Ta_3N_5, electrostatic potential of the bulk Ta_3N_5, the vacuum energy level, and the energy difference between the electrostatic potential of the Ta_3N_5 and vacuum level, respectively.

(C) The potential difference between the electrostatic potential of Ta_3N_5 and water at the Ta_3N_5-water interface.

(D) The density of water of the snapshot in an equilibrated Ta_3N_5-water unit cell.

et al., 2017; Carrasco et al., 2012; Selcuk and Selloni, 2016). For instance, the band edges of Si are shifted by approximately 0.5 eV irrespective of the termination, when it is exposed to water (Pham et al., 2014). It enlightens us to unravel the mystery of the unexpectedly high onset potentials for water oxidation over Ta_3N_5 from the view of the Ta_3N_5-water interface.

To the best of our knowledge, there have been no theoretical studies on the performances of Ta_3N_5 semiconductors in an aqueous environment. Here the effect of catalyst-water interface on the band edge potentials of Ta_3N_5 has been investigated by using DFT calculations. All the DFT and first-principles molecular dynamics (FPMD) simulations were performed by using the Vienna *ab initio* simulation package code (Kresse and Furthmüller, 1996). It is found that dissociated water can make the band edge potentials relative to vacuum shift −0.85 eV.

RESULTS

Theoretical Models and Theoretical Methods

Figure 1A shows the snapshot of the equilibrated structure for Ta_3N_5-water model. From Figure 1A, it can be observed that water partially spontaneously dissociates and results in a partial hydroxylated surface. According to previous work, water tends to dissociate to form the hydroxylated surface at certain catalyst-water interface (He et al., 2016; Held et al., 2001; Feibelman, 2002). Hence, we have considered the effect of the ratio of the dissociated water on the band edge potentials of Ta_3N_5. To illustrate the effect of catalyst-water interface on the band edge potentials of Ta_3N_5, we have calculated the band edge potentials of Ta_3N_5 not only in vacuum but also in an aqueous environment. To eliminate the underestimation of

band gap by PBE (Perdew-Burke-Ernzerhof) level, hybrid-DFT method has been used; the results of hybrid-DFT illuminated in Transparent Methods and Figure S1, are in good agreement with the experimental values (Chun et al., 2003). More detailed information is given in the Transparent Methods. For the calculations of the DFT-based molecular dynamics simulations, canonical ensemble was used and the functional optB88-vdW (Klimeš et al., 2011; Dion et al., 2004) was added to revise the long-range van der Waals interactions.

To clarify the calculation methods, a simplified schematic diagram is shown in Figures 1B and 1C. Figure 1B illustrates a two-step method to calculate the energy levels of Ta_3N_5 in vacuum. First, the bulk Ta_3N_5 model has been performed, and we can obtain the potential difference between the valence band maximum (VBM) or the conduction band minimum (CBM) and the electrostatic potential of Ta_3N_5. Second, the slab model of Ta_3N_5 in vacuum gives the potential difference between electrostatic potential of Ta_3N_5 and vacuum potential level. Therefore, the VBM or CBM of Ta_3N_5 relative to vacuum can be obtained. For the band edge potentials of catalyst in water, we have first calculated the band offset between water and catalysis. Then combining the band edge potential of water relative to vacuum, we can calculate the band edge potentials of Ta_3N_5 in water. The detailed information is shown in Figure S2 and Equation S3. The density of water along z axis in equilibrated structure for Ta_3N_5-water model is illustrated in Figure 1D. The radial distribution functions of water in Figure S4 imply that water molecules are randomly dispersed. The average density is close to 1 g/cm^3. The high mass density value of water at the two sides corresponds to the partial hydroxylated interface.

Although approaching a high photocurrent for solar water splitting (Liu et al., 2016), the low solar-to-hydrogen efficiency of Ta_3N_5 is still far below the requirements of commercial application (Bard and Fox, 1995). Previous theoretical studies on Ta_3N_5 prove that oxygen impurities and doping elements have an influence on the band edge potential of Ta_3N_5 (Fan et al., 2017; Liu et al., 2016; Wang et al., 2017). However, the working environment of Ta_3N_5 photoanode has not been considered in the previously calculated Ta_3N_5 models. The surface structure and catalytic activity of catalysts in an aqueous environment may be strikingly different from those of the catalyst in vacuum (He et al., 2016; Onda et al., 2005; Pham et al., 2014, 2017; Kharche et al., 2014). Whether the high onset potential of Ta_3N_5 is relative to an aqueous working environment is what we want to investigate in this study. The calculated band edge potentials of Ta_3N_5-water interface are the average values of 13 equilibrated Ta_3N_5-water unit cells (see Transparent Methods, Figure S3). Thirteen unit cells are enough for the required precision because the variations of the average band edge potential values of 9, 11, and 13 unit cells are smaller than 0.05 eV.

Calculations of Band Edge Positions

Figure 2 displays the band edge potential of Ta_3N_5 relative to vacuum in different conditions. The HSE (Heyd-Scuseria-Ernzerhof) revised band gap of Ta_3N_5 is 2.14 eV, which is very close to experimental values (Chun et al., 2003; Liu et al., 2016; Li et al., 2013a, 2013b). The VBM and CBM of Ta_3N_5 relative to vacuum are calculated to be −6.30 and −4.16 eV, respectively. It is well known that the relationship between the absolute potential relative to vacuum and a normal hydrogen electrode (NHE) at 298 K can be shown as follows:

$$E_{vac} = -E_{NHE} - 4.44 \quad \text{(Equation 1)}$$

Therefore, the VBM and CBM of Ta_3N_5 are equal to 1.86 and −0.28 V versus NHE, respectively. This implies that the VBM is more positive than the water oxidation potential and the CBM is more negative than water reduction potential versus NHE. Subsequently, the band edge potentials of Ta_3N_5 in vacuum indicate that Ta_3N_5 can split water without any external bias. It may be an ideal photoelectrode for water splitting. Nevertheless, water splitting for a single Ta_3N_5 photoanode without external bias has been not achieved experimentally yet. External bias of 0.6–0.9 V is always required for photoelectrochemical water oxidation over single Ta_3N_5 photoanodes even if they are loaded by OER electrocatalysts. This may arise from the fact that Ta_3N_5 behaves differently in an aqueous environment.

Figure 2 also shows that both aqueous environment and the ratio of dissociated water will shift the band edge potentials negatively relative to vacuum level, which is in agreement with the results from PBE level (see Figure S5). The negative shifts of the band edge potentials are harmful to the onset potential of Ta_3N_5 photoanodes because the counterelectrode needs more external bias to drive the water reduction reaction. Therefore, the negative shifts of band edge potentials of Ta_3N_5 can increase the onset potential for water oxidation, thus reducing the solar-to-hydrogen efficiency of Ta_3N_5. Comparing the band edge

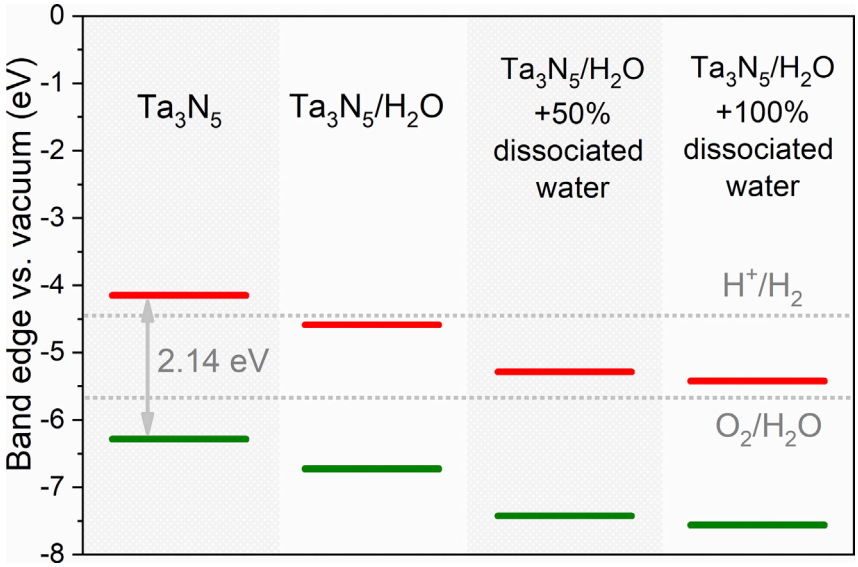

Figure 2. Band Edge Potentials

The calculated band edge potentials of the bulk Ta_3N_5, Ta_3N_5-water interface, Ta_3N_5-water interface with 50% dissociated interfacial water, and full hydroxylated Ta_3N_5-water interface relative to vacuum. The gray dashed lines are the water reduction and oxidation potentials, respectively.

potentials of Ta_3N_5 in vacuum with those at the Ta_3N_5-H_2O interface, we can find that when exposed to water, the band edge potential relative to vacuum shifts −0.42 eV. The ratio of dissociated water also has a great influence on the band edge potentials of Ta_3N_5. When we intentionally build the Ta_3N_5 models with 50% and 100% initial hydroxylated interface, their band edge potentials relative to vacuum shift −0.72 and −0.85 eV compared with the Ta_3N_5-H_2O model, respectively. It indicates that the ratio of dissociated water has an important effect on the band edge potentials. From Figure 1A, we can find that water and hydroxide are bonded to Ta atoms, whereas N sites are protonated. Our previous study (Wang et al., 2013) has also suggested that the single dissociated water on the Ta_3N_5 (1 0 0) surface tends to gain electrons.

Charge Transfer Calculations

To understand the surface charge transfer property, the one-dimensional (1D) charge density difference along z axis shown in Figure 3 is defined as follows:

$$\Delta\rho_e = \Delta\rho_e^{cat/wat} - \Delta\rho_e^{cat} - \Delta\rho_e^{wat} \quad \text{(Equation 2)}$$

where $\Delta\rho_e{}^{cat/wat}$, $\Delta\rho_e{}^{cat}$, and $\Delta\rho_e{}^{wat}$ are the charge densities of Ta_3N_5-water unit cell, Ta_3N_5 slab model, and water unit cell, respectively.

Figure 3 demonstrates that both the water and the dissociated water at the Ta_3N_5-water interface gain electrons, whereas the surface Ta_3N_5 layer loses electrons. This means that the electrons transfer from Ta_3N_5 to water, that is, the Ta_3N_5 surface layer may form an additional surface dipole. Similar surface dipole has also appeared in Si, GaN, and ZnO semiconductors when exposed to water (Pham et al., 2014; Kharche et al., 2014). To quantify the charge transfer at the surface, the integrals of the 1D charge density have been performed (see Figures S6–S9). Figure S6 suggests that the hydroxylated surface facilitates the electron transfer from Ta_3N_5 surface to water at the interface, implying that both the ratio of dissociated water at the interface and the aqueous environment have a significant effect on the formation of surface dipole and surface oxidation of Ta_3N_5 at the Ta_3N_5-water interface.

Bader Charge Analysis

To further confirm the charge transfer process, bader charge analysis of Ta_3N_5-water has been performed. The total and average charges of Ta and N atoms in the surface layer are exhibited in Table 1. According to Table 1, the total electrons of the surface Ta_3N_5 layer decrease when exposed in an aqueous environment

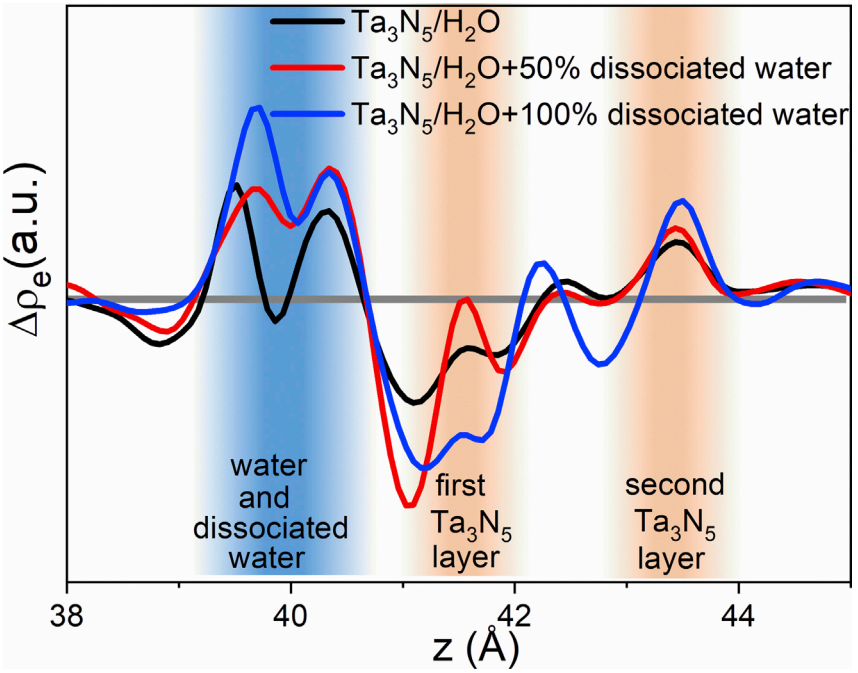

Figure 3. Charge Transfer in the Ta_3N_5-Water Interface

The positive values represent the addition of the electrons, whereas the negative values imply the donation of electrons. The blue area corresponds to the water at the interface. Meanwhile, the orange area corresponds to the surface Ta_3N_5 layer and the subsurface Ta_3N_5 layer.

and further decrease with the increase of the dissociated water ratio. This clearly demonstrates that when exposed to water surface Ta_3N_5 layer acts as electron donor and the increase of hydroxylated ratio accelerates the electron transfer from the surface Ta_3N_5 layer to water at the interface. As well known, for an ideal photoanode, the photoinduced holes instead of electrons should transfer from its surface layer to water at the interface, and then take part in the reaction of water oxidation. Obviously, the electron transfer from the surface Ta_3N_5 layer to water will lead to recombination of electrons and holes at the interface, which also reduces their PEC performance for water splitting. The surface dipole shown in Figure 3 will lead to a negative shift of band edge potentials of Ta_3N_5 relative to vacuum.

Table 1 also reveals that the variation of the total charge of N atoms is opposite to that of Ta atoms. Nonetheless, the absolute change of charge transfer of Ta is much greater than that of N atoms, which may favor the oxidation of the Ta_3N_5 surface layer. A Ta_2O_5 amorphous nanometer layer on the surface of Ta_3N_5 photoanodes has been observed after PEC water oxidation (He et al., 2016). In our experiments, the carrier concentration of Ta_3N_5 photoanodes has been found to become smaller during the process of PEC water oxidation, which may be due to the surface oxidation of Ta_3N_5. Combining charge density difference and bader charge analysis, we may conclude that the aqueous environment and the hydroxylated surface promote the formation of dipole at the interface and even the surface oxidation of Ta_3N_5 photoanodes. Facet and co-catalyst play important roles in real water splitting system; Figures S10–S12 show the effects of facet and co-catalyst (or co-catalyst) on the shifts of band edge potentials. According to these figures, the facet, the termination of facet, and different co-catalysts or overlayer have a great influence on the charge transfer at interface, and therefore affect the shift in band edge potentials.

DISCUSSION

As discussed above, Ta_3N_5-water interface has a great influence on the band edge potentials and stability. The common strategy to overcome these problems is to tune the surface electronic structure by coating an overlayer or loading co-catalysts. Recently, a GaN overlayer has been proved to favor the onset potential for water oxidation and improve photochemical stability of Ta_3N_5, due to the restriction of the formation of self-oxidation surfaces (Zhong et al., 2017). However, the deposition of OER co-catalysts, such as Co_3O_4

Charge Transfer/Electrons[a]	Ta_3N_5-Water	Ta_3N_5-Water with 50% Dissociated Water	Ta_3N_5-Water with 100% Dissociated Water
Total charge transfer of Ta	−1.22	−1.52	−1.72
Average charge transfer Ta	−0.10	−0.13	−0.14
Total charge transfer of N	0.12	0.23	0.40
Average charge transfer N	0.01	0.01	0.02

Table 1. Bader Charge Analysis of Ta3N5-Water Unit Cells

[a]The total charge transfer is the difference between the total bader charges of all the surface Ta or N atoms in water and the total bader charges of the surface Ta or N atoms in vacuum. The average charge transfer is the average electron transfer of per Ta or N atom in the surface. The bader charge of a surface Ta atom and N atom in vacuum are 2.76 and 6.35, respectively. There are 12 surface Ta atoms and 20 surface N atoms in all models.

(Liao et al., 2012), NiFe layered double hydroxide (Wang et al., 2015a, 2015b), $Ni(OH)_x$ (Liu et al., 2016), and IrO_2 (Higashi et al., 2011), have limited effect on the onset potential performances of Ta_3N_5 photoanodes. The effect of termination in Figure S11 suggests that it is worthwhile to optimize the methods to deposit the co-catalysts, because the nanostructure of co-catalysts (Seger et al., 2013; Ping et al., 2015) as well as the experimental parameters (Paracchino et al., 2012) will influence the electronic environment and the catalyst-water interface. Therefore, interface engineering is a promising way to enhance the performance of Ta_3N_5 by regulating the electronic structure at the catalyst-water interface and restricting the oxidation of Ta_3N_5 surface. The investigation of the mechanism of water oxidation under illumination at Ta_3N_5-electrolyte interface is meaningful, because it is generally accepted that the photogenerated holes will oxidize the surface Ta_3N_5 and generate N_2 (Liao et al., 2012). However, this dynamic oxidation process at Ta_3N_5-electrolyte interface is still unclear. Combining theory and *in situ* experiments (Herlihy et al., 2016) is a promising strategy to investigate the dynamic process of water oxidation at the Ta_3N_5-water interface under illumination.

In conclusion, the DFT and FPMD simulations were performed to investigate the band edge behavior of Ta_3N_5 in an aqueous environment. The HSE revised band gaps and band edge potentials of Ta_3N_5 are close to the experimental values. The band edge potentials of Ta_3N_5 are found to shift negatively relative to vacuum level when exposed to water. The negative shift is harmful to the onset potential performance of Ta_3N_5 photoanodes. The negative significant shift of the band edge positions may explain why a bias of at least 0.6–0.7 V_{REH} should be applied for water splitting over Ta_3N_5 photoanodes. Facet, termination of facet, and co-catalyst will also affect the shift of the band edge positions of Ta_3N_5. Interface engineering, as well as defect engineering (Feng et al., 2019), is a promising way to improve photoelectrochemical performances for water splitting over photoanodes.

Limitations of the Study

This study demonstrates the effect of water on the shifts of band edge potentials of Ta_3N_5. We also consider the effect of co-catalyst or overlayer on the shifts of band edge potentials. However, water-overlayer (or co-catalyst)-Ta_3N_5 in real Ta_3N_5 photoelectrochemical water splitting system is very complex for DFT calculation. Therefore the development of a more complex model that can accurately describe the real water splitting system will be necessary.

METHODS

All methods can be found in the accompanying Transparent Methods supplemental file.

SUPPLEMENTAL INFORMATION

Supplemental Information can be found online at https://doi.org/10.1016/j.isci.2019.02.024.

ACKNOWLEDGMENTS

This work was supported by National Key Research and Development Program of China (No: 2018YFA0209303), the National Natural Science Foundation of China (Nos: U1663228 and 21473090),

and a project funded by the Priority Academic Program Development of Jiangsu Higher Education Institutions. The authors are also grateful to the High Performance Computing Center (HPCC) of Nanjing University for allowing use of its IBM Blade cluster system for the numerical calculations discussed in this study.

AUTHOR CONTRIBUTIONS

G.F. and Z.L. conceived the study and co-wrote the manuscript. G.F. carried out the theoretical calculations. T.F., X.W., Y.Z., H.F., J.F., and Z.Z. helped with manuscript preparation.

DECLARATION OF INTERESTS

The authors declare no competing interests.

Received: October 1, 2018
Revised: January 29, 2019
Accepted: February 24, 2019
Published: March 29, 2019

REFERENCES

Bard, A.J., and Fox, M.A. (1995). Artificial photosynthesis: solar splitting of water to hydrogen and oxygen. Acc. Chem. Res. *28*, 141–145.

Carrasco, J., Hodgson, A., and Michaelides, A. (2012). A molecular perspective of water at metal interfaces. Nat. Mater. *11*, 667–674.

Chen, Z., Dinh, H., and Miller, E. (2013). Photoelectrochemical Water Splitting (Springer), pp. 7–16.

Chen, Q., Fan, G., Fu, H., Li, Z., and Zou, Z. (2018). Tandem photoelectrochemical cells for solar water splitting. Adv. Phys.X *3*, 1487267.

Chun, W.-J., Ishikawa, A., Fujisawa, H., Takata, T., Kondo, J.N., Hara, M., Kawai, M., Matsumoto, Y., and Domen, K. (2003). Conduction and valence band positions of Ta_2O_5, TaON, and Ta_3N_5 by UPS and electrochemical methods. J. Phys. Chem. B *107*, 1798–1803.

Dion, M., Rydberg, H., Schröder, E., Langreth, D.C., and Lundqvist, B.I. (2004). Van der Waals density functional for general geometries. Phys. Rev. Lett. *92*, 246401.

Fan, G., Wang, X., Fu, H., Feng, J., Li, Z., and Zou, Z. (2017). Compensation of band-edge positions in titanium-doped Ta_3N_5 photoanode for enhanced water splitting performance: a first-principles insight. Phys. Rev. Mater. *1*, 035403.

Feibelman, P.J. (2002). Partial dissociation of water on Ru (0 0 0 1). Science *295*, 99–102.

Feng, J., Huang, H., Fang, T., Wang, X., Yan, S., Luo, W., Yu, T., Zhao, Y., Li, Z., and Zou, Z. (2019). Defect engineering in semiconductors: manipulating nonstoichiometric defects and understanding their impact in oxynitrides for solar energy conversion. Adv. Funct. Mater. *29*, https://doi.org/10.1002/adfm.201808389.

He, Y., Thorne, J., Wu, C., Ma, P., Du, C., Dong, Q., Guo, J., and Wang, D. (2016). What limits the performance of Ta_3N_5 for solar water splitting? Chem *1*, 640–655.

Held, G., Braun, W., Steinrück, H.P., Yamagishi, S., Jenkins, S.J., and King, D.A. (2001). Light-atom location in adsorbed benzene by experiment and theory. Phys. Rev. Lett. *87*, 216102.

Herlihy, D.M., Waegele, M.M., Chen, X., Pemmaraju, C.D., Prendergast, D., and Cuk, T. (2016). Detecting the oxyl radical of photocatalytic water oxidation at an n-$SrTiO_3$/aqueous interface through its subsurface vibration. Nat. Chem. *8*, 549–555.

Higashi, M., Domen, K., and Abe, R. (2011). Fabrication of efficient TaON and Ta_3N_5 photoanodes for water splitting under visible light irradiation. Energy Environ. Sci. *4*, 4138–4147.

Hu, S., Xiang, C., Haussener, S., Berger, A.D., and Lewis, N.S. (2013). An analysis of the optimal band gaps of light absorbers in integrated tandem photoelectrochemical water-splitting systems. Energy Environ. Sci. *6*, 2984–2993.

Hu, Z., Li, Q., Lei, B., Zhou, Q., Xiang, D., Lyu, Z., Hu, F., Wang, J., Ren, Y., Guo, R., et al. (2017). Water-catalyzed oxidation of few-layer black phosphorous in a dark environment. Angew. Chem. Int. Ed. *56*, 9131–9135.

Kharche, N., Muckerman, J.T., and Hybertsen, M.S. (2014). First-principles approach to calculating energy level alignment at aqueous semiconductor interfaces. Phys. Rev. Lett. *113*, 176802.

Klimeš, J., Bowler, D.R., and Michaelides, A. (2011). Van der Waals density functionals applied to solids. Phys. Rev. B *83*, 195131.

Kresse, G., and Furthmüller, J. (1996). Efficient iterative schemes for ab initio total-energy calculations using a plane-wave basis set. Phys. Rev. B *54*, 11169–11186.

van de Krol, R., and Grätzel, M. (2012). Photoelectrochemical Hydrogen Production, *2012* (Springer), pp. 36–44.

Li, Z., Luo, W., Zhang, M., Feng, J., and Zou, Z. (2013a). Photoelectrochemical cells for solar hydrogen production: current state of promising photoelectrodes, methods to improve their properties, and outlook. Energy Environ. Sci. *6*, 347–370.

Li, M., Luo, W., Cao, D., Zhao, X., Li, Z., Yu, T., and Zou, Z. (2013b). A Co-catalyst-loaded Ta_3N_5 photoanode with a high solar photocurrent for water splitting upon facile removal of the surface layer. Angew. Chem. Int. Ed. *52*, 11016–11020.

Li, Z., Feng, J., Yan, S., and Zou, Z. (2015). Solar fuel production: strategies and new opportunities with nanostructures. Nano Today *10*, 468–486.

Liao, M., Feng, J., Luo, W., Wang, Z., Zhang, J., Li, Z., Yu, T., and Zou, Z. (2012). Co_3O_4 nanoparticles as robust water oxidation catalysts towards remarkably enhanced photostability of a Ta_3N_5 photoanode. Adv. Funct. Mater. *22*, 3066–3074.

Liu, G., Ye, S., Yan, P., Xiong, F., Fu, P., Wang, Z., Chen, Z., Shi, J., and Li, C. (2016). Enabling an integrated tantalum nitride photoanode to approach the theoretical photocurrent limit for solar water splitting. Energy Environ. Sci. *9*, 1327–1334.

Onda, K., Li, B., Zhao, J., Jordan, K., Yang, J., and Petek, H. (2005). Wet electrons at the H_2O/TiO_2(110) surface. Science *308*, 1154–1158.

Paracchino, A., Mathews, N., Hisatomi, T., Stefik, M., Tilley, S.D., and Grätzel, M. (2012). Ultrathin films on copper(I) oxide water splitting photocathodes: a study on performance and stability. Energy Environ. Sci. *5*, 8673–8681.

Pham, T., Lee, D., Schwegler, E., and Galli, G. (2014). Interfacial effects on the band edges of functionalized Si surfaces in liquid water. J. Am. Chem. Soc. *136*, 17071–17077.

Pham, T., Ping, Y., and Galli, G. (2017). Modelling heterogeneous interfaces for solar water splitting. Nat. Mater. *16*, 40–408.

Ping, Y., Goddard, W., and Galli, G. (2015). Energetics and solvation effects at the photoanode/catalyst interface: ohmic contact versus Schottky barrier. J. Am. Chem. Soc. *137*, 5264–5267.

Seger, B., Pedersen, T.S., Laursen, A.B., Vesborg, P.C.K., Hansen, O., and Chorkendorff, I. (2013). Using TiO_2 as a conductive protective layer for photocathodic H_2 evolution. J. Am. Chem. Soc. *135*, 1057–1064.

Selcuk, S., and Selloni, A. (2016). Facet-dependent trapping and dynamics of excess electrons at anatase TiO_2 surfaces and aqueous interfaces. Nat. Mater. *15*, 1107–1112.

Seo, J., Takata, T., Nakabayashi, M., Hisatomi, T., Shibata, N., Minegishi, T., and Domen, K. (2015). Mg–Zr cosubstituted Ta_3N_5 photoanode for lower-onset-potential solar-driven photoelectrochemical water splitting. J. Am. Chem. Soc. *137*, 12780–12783.

Wang, J., Luo, W., Feng, J., Zhang, L., Li, Z., and Zou, Z. (2013). Theoretical study of water adsorption and dissociation on Ta_3N_5 (1 0 0) surfaces. Phys. Chem. Chem. Phys. *15*, 16054–16064.

Wang, J., Fang, T., Zhang, L., Feng, J., Li, Z., and Zou, Z. (2014). Effects of oxygen doping on optical band gap and band edge positions of Ta_3N_5 photocatalyst: a GGA plus U calculation. J. Catal. *309*, 291–299.

Wang, J., Ma, A., Li, Z., Jiang, J., Feng, J., and Zou, Z. (2015a). Effects of oxygen impurities and nitrogen vacancies on the surface properties of the Ta_3N_5 photocatalyst: a DFT study. Phys. Chem. Chem. Phys. *17*, 23265–23272.

Wang, L., Dionigi, F., Nguyen, N.T., Kirchgeorg, R., Gliech, M., Grigorescu, S., Strasser, P., and Schmuki, P. (2015b). Tantalum nitride nanorod arrays: introducing Ni-Fe layered double hydroxides as a cocatalyst strongly stabilizing photoanodes in water splitting. Chem. Mater. *27*, 2360–2366.

Wang, L., Zhou, X., Nguyen, N., Hwang, I., and Schmuki, P. (2016). Strongly enhanced water splitting performance of Ta_3N_5 nanotube photoanodes with subnitrides. Adv. Mater. *28*, 2432–2438.

Wang, J., Ma, A., Li, Z., Jiang, J., Chen, J., and Zou, Z. (2017). Effects of Mg–Zr codoping on the photoelectrochemical properties of a Ta_3N_5 semiconductor: a theoretical insight. J. Mater. Chem. A *5*, 6966–6973.

Zhang, P., Wang, T., and Gong, J. (2016). Passivation of surface states by ALD-grown TiO_2 overlayers on Ta_3N_5 anodes for photoelectrochemical water oxidation. Chem. Commun. *52*, 8806–8809.

Zhong, M., Hisatomi, T., Sasaki, Y., Suzuki, S., Teshima, K., Nakabayashi, M., Shibata, N., Nishiyama, H., Katayama, M., Yamada, T., and Domen, K. (2017). Highly active GaN-stabilized Ta_3N_5 thin-film photoanode for solar water oxidation. Angew. Chem. Int. Ed. *56*, 4739–4743.

ISCI, Volume *13*

Supplemental Information

Interfacial Effects on the Band Edges of Ta_3N_5 Photoanodes in an Aqueous Environment: A Theoretical View

Guozheng Fan, Tao Fang, Xin Wang, Yaodong Zhu, Hongwei Fu, Jianyong Feng, Zhaosheng Li, and Zhigang Zou

Supplemental Information

Interfacial Effects on the Band Edges of Ta_3N_5 Photoanodes in an Aqueous Environment: a Theoretical View

Guozheng Fan, [1] Tao Fang, [1] Xin Wang, [1] Yaodong Zhu, [1] Hongwei Fu, [1] Jianyong Feng, [1] Zhaosheng Li, [1, 2, 3, *] Zhigang Zou [1,2]

[1] Collaborative Innovation Center of Advanced Microstructures, National Laboratory of Solid State Microstructures, College of Engineering and Applied Sciences, Nanjing University, Nanjing 210093, P. R. China.

[2] Jiangsu Key Laboratory for Nano Technology, Nanjing University, Nanjing 210093, P. R. China.

[3] Lead Contact

Correspondence: zsli@nju.edu.cn (Z. L.)

Transparent Methods

Band Edge Calculations Methods

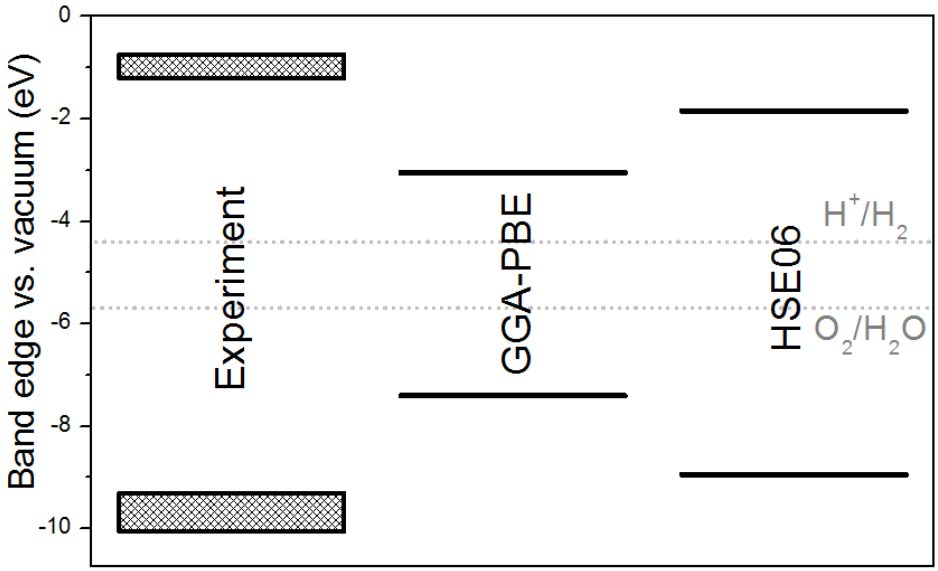

Figure S1. Band edge potentials, related to Figure 1.

The calculated band edge potentials water and the experiments values of water from reference.[1]

Figure S1 shows the band edge potentials of water relative to vacuum based on GGA-PBE method and HSE method. Figure S1 demonstrates that the band edge potentials of water using HSE method are close to the experimental values, suggesting that HSE method can revise the band gap and band edge potentials effectively.

The method of band edge potentials for Ta_3N_5 in vacuum has been shown in Figure S2 and Figure 1. We have calculated the band edge potentials of Ta_3N_5 in vacuum by two steps. Firstly, the bulk Ta_3N_5 model have been calculated. Thus, we can obtain the potential difference between VBM or CBM and electrostatic potential of bulk Ta_3N_5. Secondly, the slab model of Ta_3N_5 in vacuum has been performed and the slab model gives the potential difference between electrostatic potential of bulk Ta_3N_5 and vacuum potential level. Therefore, the VBM of Ta_3N_5 relative to vacuum potential can be obtained. Both band edge potentials calculated from PBE and HSE06 can be obtained from equation S2:

$$VBM_{cat}^{vac} = VBM_{VBM}^{bulk} + \Delta V_{bulk}^{vac} \qquad (1)$$

Here, taking the VBM of Ta_3N_5 as an example, VBM_{cat}^{vac} is the VBM of Ta_3N_5 (catalyst) versus vacuum potential level; VBM_{VBM}^{bulk} is the potential difference between the

calculated VBM and electrostatic potential in bulk Ta_3N_5 model. ΔV_{bulk}^{vac} is the potential difference between electrostatic potential of Ta_3N_5 and the vacuum potential level in slab model of Ta_3N_5.

For the band edge potentials of catalyst in water, we calculate band offset between water and the catalysis at first. Then combining the band edge potentials of water relative to vacuum, we can calculate the band potentials of Ta_3N_5 in water. Figure 1c gives the schematic diagram of the line term. The entire valence band alignment calculation procedure is shown as shown in Figure S2:

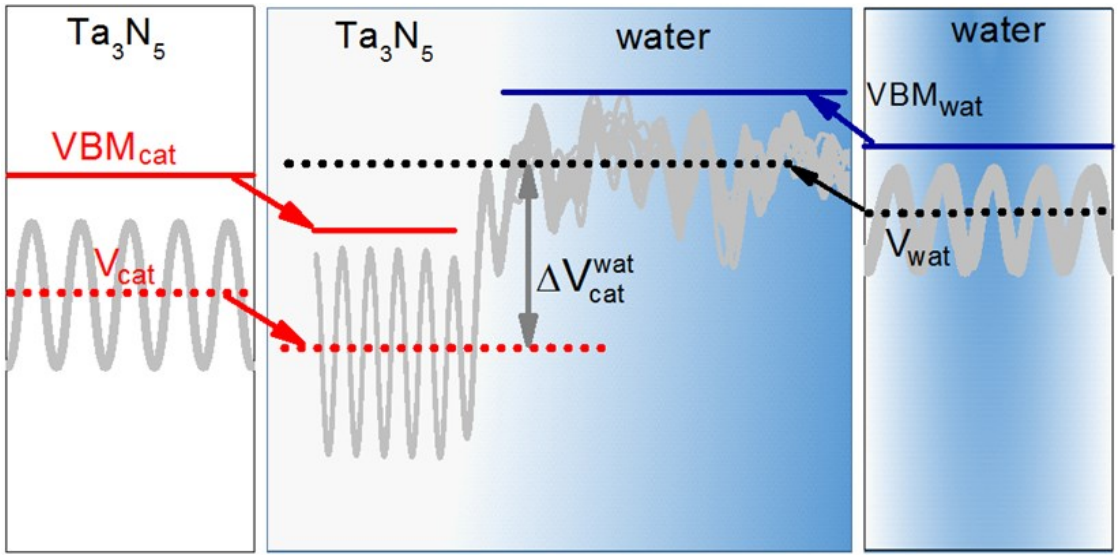

Figure S2. Calculation Method, related to Figure 1.

Simplified schematic diagram of the band potential of Ta_3N_5 in an aqueous environment.

Figure S2 can be expressed as follows:

$$\Delta VBM_{cat}^{wat} = \langle VBM_{cat} - V_{cat} \rangle - \langle VBM_{wat} - V_{wat} \rangle + \langle \Delta V_{cat}^{wat} \rangle_{int} \qquad (2)$$

here, ΔVBM_{cat}^{wat} is the calculated valence band alignment of VBM of Ta_3N_5 in water. VBM_{wat} is the potential of VBM of water. V_{wat} is electrostatic potential of water. To eliminate the electrostatic potential difference between Ta_3N_5 and water, the line up term $\langle \Delta V_{cat}^{wat} \rangle_{int}$ should be added, which is illustrated in Figure 1c and Figure S2. From Figure S2,we can calculate the valence band alignment, then combining the VBM of water, we can get the VBM of Ta_3N_5 in water.

Calculation methods details

Firstly, for the DFT calculation part, the exchange correlation potential is calculated with the projected-augmented-wave (PAW) method[2] in the scheme of Perdew-Bueke-

Ernzerhof (PBE) functional.[3, 4] To revise the bandgap value from PBE-based calculations, hybrid-DFT calculations are used[5, 6] in the scheme of Heyd-Scuseria-Ernzerhof (HSE) functional.[6] The HSE06 functional is adopted, demonstrating that the two critical parameters of hybrid-DFT calculations, mixing parameter α and screening parameter ω, are 25% and 0.2 Å $^{-1}$, respectively.[6] The cutoff energies for all calculations are 500 eV and have been tested enough for the computational accuracy.[7] The relaxed lattice constant parameters of bulk Ta_3N_5 (a = 3.95 Å, b = 10.23 Å, and c = 10.30 Å) are in good agreement with experimental values[8] (a = 3.88 Å, b = 10.21 Å, and c = 10.26 Å), suggesting that the calculations are reliable. The 3 × 1 × 1 conventional bulk Ta_3N_5 supercells are chosen (space group: Cmcm) to use 2 × 2 × 2 K meshes. For the slab model of Ta_3N_5, a vacuum space of 15 Å is added. For all TiO_2 systems and Ta_3N_5-co-catalyst systems, PBE method was adpoted.

Secondly, for the Ta_3N_5-water and TiO_2-water interfaces calculations, DFT-based MD calculations have been performed. The cutoff energy is 500 eV and the temperature is 300 K by a Nose-Hoover thermostat.[9, 10] The line term are obtained from NVT simulations by calculating the average electrostatic potentials of 13 snapshots. Thirteen snapshots is enough for the accuracy of band edge potentials, as is shown in Figure S3.

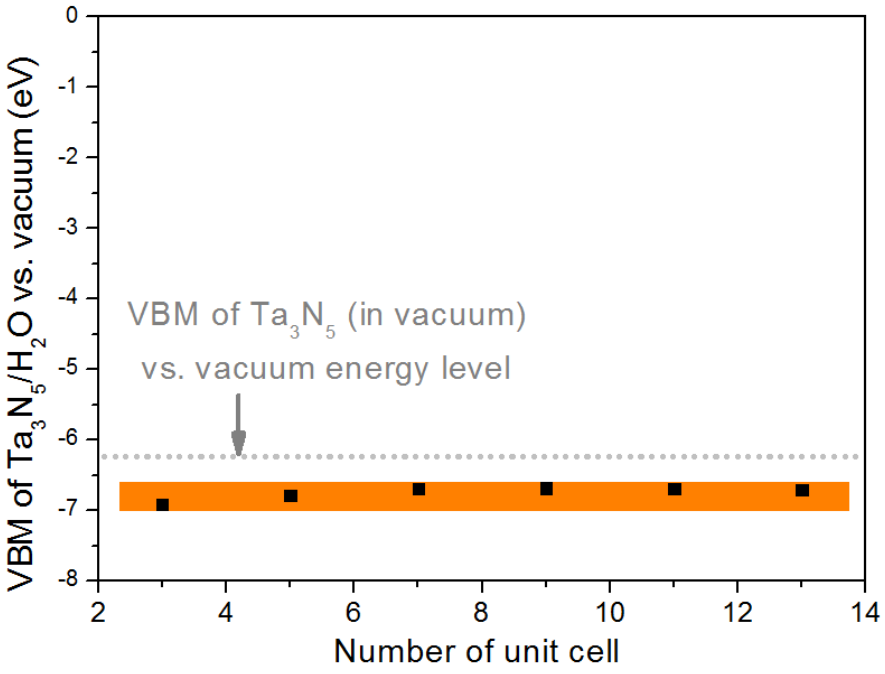

Figure S3. Effect of number of snapshots on the band edge potentials, related to Figure 1. The average band edge potentials of Ta_3N_5. The x axis represent the number of snapshots extracted from ab initio MD simulations.

1. Radial distribution functions (RDF)

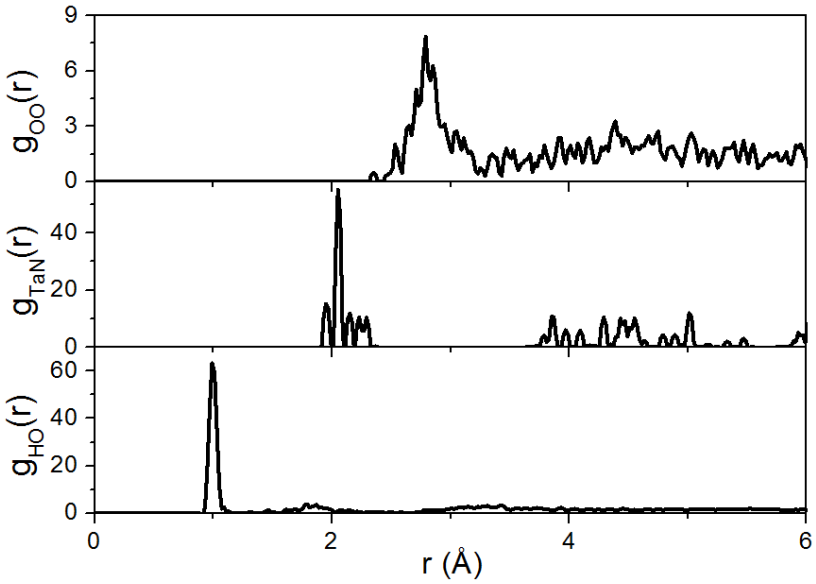

Figure S4. RDF, related to Figure 1.

The RDF of O-O, Ta-N and H-O bands.

The RDF shown in Figure S4 gives the information about the atomic bond lengths as well as the degree of order and polymerization. The RDF can be mathematically expressed as follows:

$$g_{AB}(r) = 4\pi r^2 \rho dr \qquad (3)$$

where ρ is the number density of B, and r is the distance away from the particle A.

2. Band edge potentials and band alignment at the interface

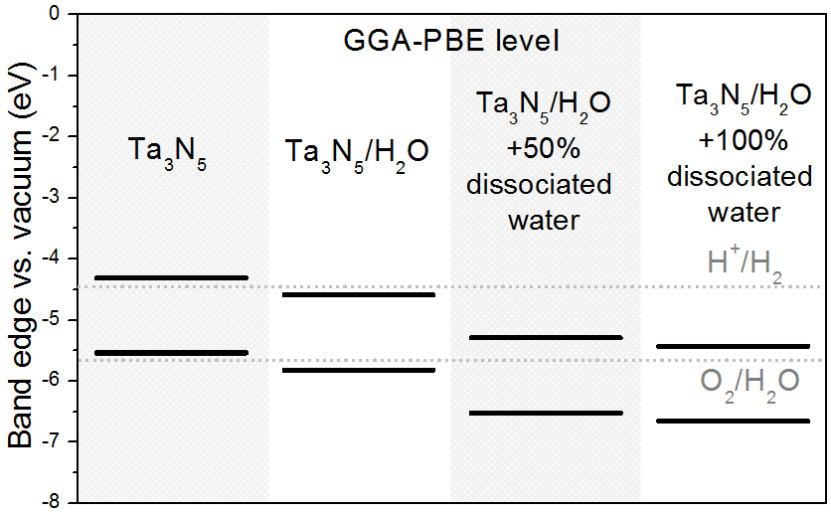

Figure S5. The band edge potentials, related to Figure 2.

The calculated band edge potentials of the Ta_3N_5 in vacuum, Ta_3N_5-water interface, Ta_3N_5-water interface with 50% dissociated interfacial water and full hydroxylated Ta_3N_5-water interface, respectively. The grey lines are the water reduction and oxidation potential respectively. The calculations are based on GGA-PBE exchange correlation Potential.

Figure S5 shows the band edge potentials of Ta_3N_5 in vacuum as well as in an aqueous environment with different water dissociated ratios. The results in Figure S5 are in a good agreement with the results shown in Figure 2. Figure S5 implies that the band edge potentials of Ta_3N_5 shift negatively relative to vacuum when exposed to water. Besides, the increased dissociated water ratio contributes to the further negative shifts of the band edge potentials of Ta_3N_5 relative to vacuum. This indicates that the calculations of the band edge potentials of Ta_3N_5 are reliable.

3. Charge transfer properties at the interface

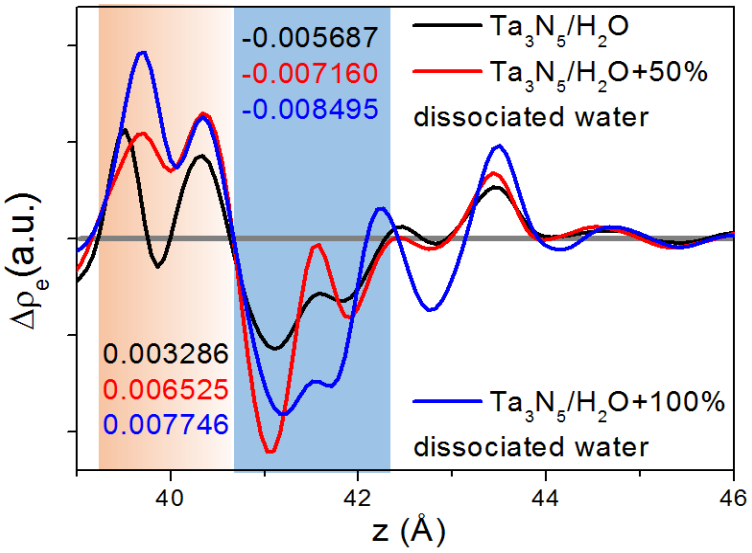

Figure S6. Charge transfer, related to Figure 3.

Charge transfer along z-axis at the Ta_3N_5-water interface, Ta_3N_5-water interface with 50% dissociated interfacial water and full hydroxylated Ta_3N_5-water interface. The positive values represent the addition of the electrons while negative value imply the donation of electrons. The blue and orange area corresponds to the range of integration. The integral values are shown in Figure S6 with different color.

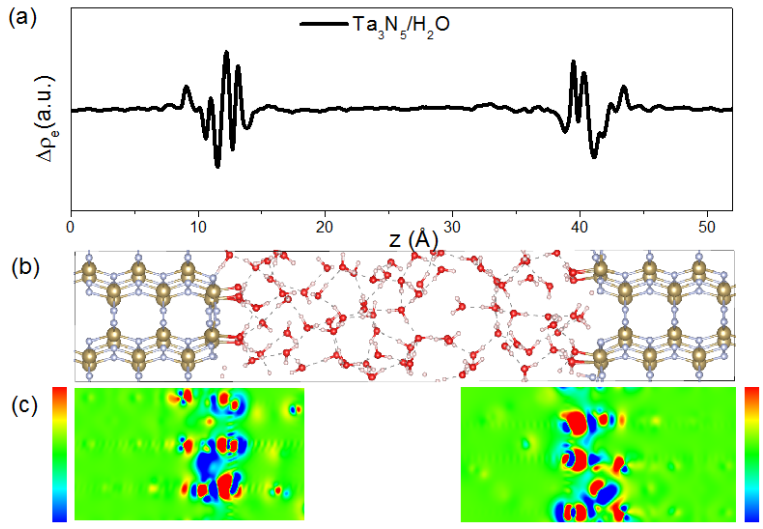

Figure S7. Charge transfer, related to Figure 3.

(a) 1D Charge transfer along z-axis at the Ta_3N_5-water interface.

(b) Corresponding atomic structure of the snapshot of equilibrated Ta_3N_5-water unit cell.

(c) 2D Charge transfer along z-axis at the Ta_3N_5-water interface. The blue and red areas correspond to electron increase and electron decrease.

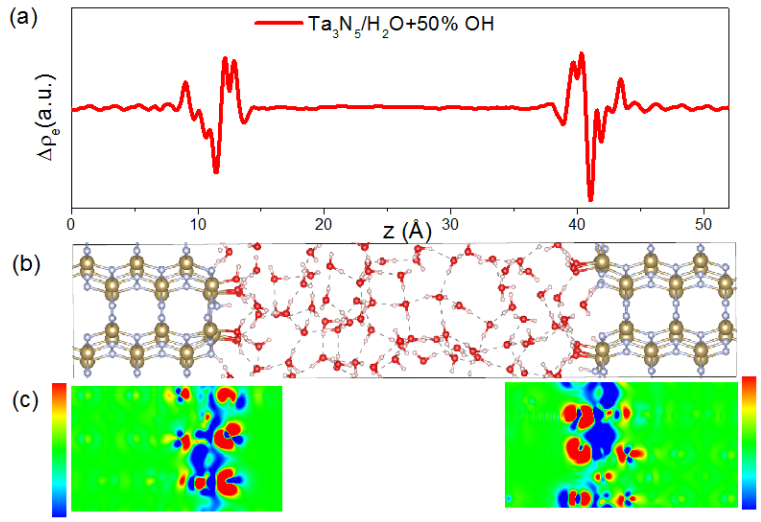

Figure S8. Charge transfer, related to Figure 3.

(a) 1D Charge transfer along z-axis at the Ta_3N_5-water interface with 50% dissociated interfacial water.

(b) Corresponding atomic structure of the snapshot of equilibrated Ta_3N_5-water with 50% dissociated interfacial water unit cell.

(c) 2D Charge transfer along z-axis at the Ta_3N_5-water interface. The blue and red areas correspond to electron increase and electron decrease.

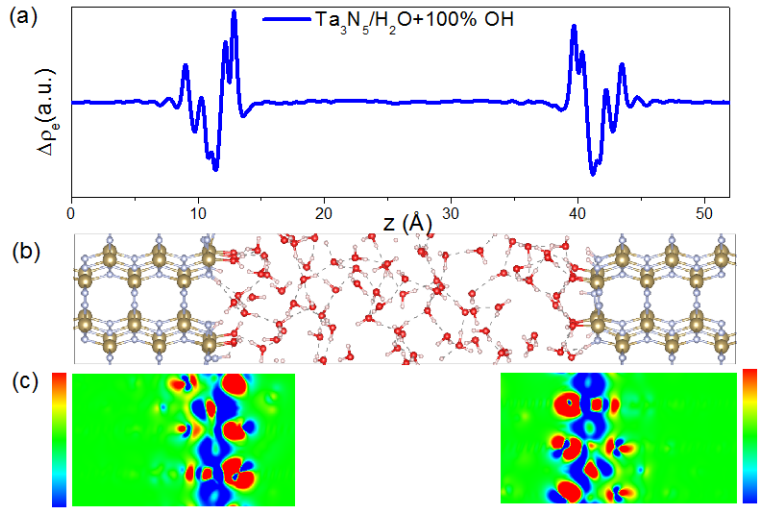

Figure S9. Charge transfer, related to Figure 3.

(a) 1D Charge transfer along z-axis at the Ta_3N_5-water interface with full hydroxylated interface.

(b) Corresponding atomic structure of the snapshot of equilibrated Ta_3N_5-water with full hydroxylated unit cell.

(c) 2D Charge transfer along z-axis at the Ta_3N_5-water interface. The blue and red areas correspond to electron increase and electron decrease.

4. Effects of co-catalyst (or overlayer) and facet on the bandgap potentials

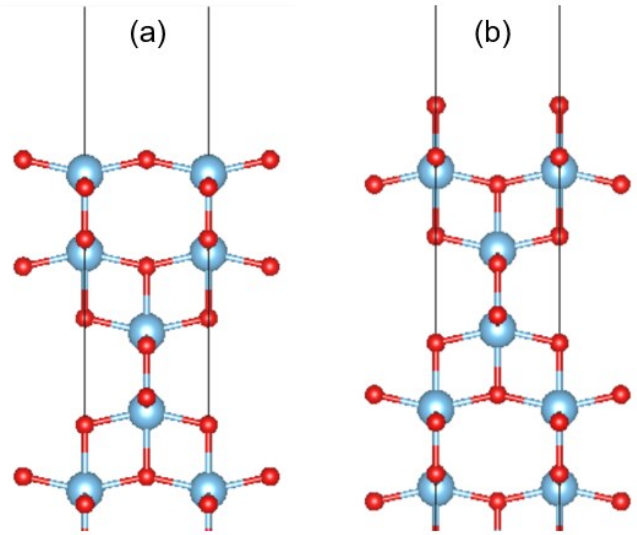

Figure S10. TiO_2 surface configuration, related to Figure 3.

Two different terminations of TiO_2 (001) orientation. (a) is TiO_2 $(001)_1$ and (b) is TiO_2 $(001)_2$.

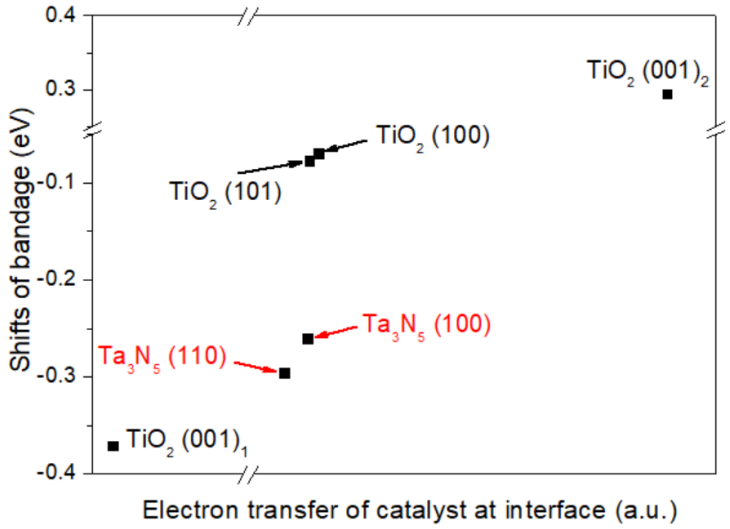

Figure S11. The shifts of band edge potentials, related to Figure 3.

The effects of different facet and different terminations of facets on the shifts of bandgap potentials in catalyst-water systems.

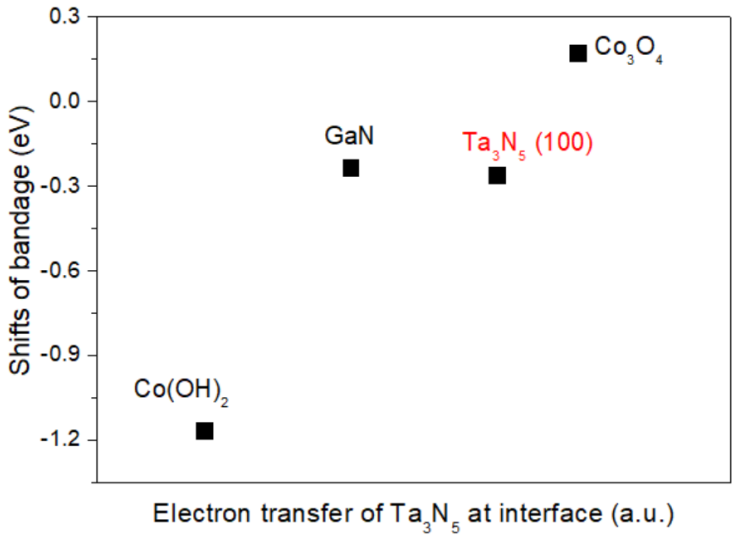

Figure S12. The shifts of band edge potentials, related to Figure 3.

The effects of different co-catalysts and overlayer on the shifts of band edge potentials of Ta_3N_5. Ta_3N_5 (100) represents Ta_3N_5 (100) facet and water interface.

The (110) orientation has exhibited the improved photoelectrochemical activities according to recent experimental and theoretical calculations.[11, 12] Therefore, we firstly compare the (100) and (110) facets. From Figure S10, we can conclude that the more electron transfer from Ta_3N_5 (100) or (110) surface layer, the more negative shifts of the bandgap potantial. To verify the influece of facets, we have performed calculations of different facets of TiO_2. Because the (001) facet of TiO_2 have different terminations, the effect of terminations have also been taken into consideration. Figure S11 implies that different facets and the terminations will greatly influence the charge transfer at interface, and the charge tranfer has a strong effect on the shifts of bandgap potentials.

Catalyst/co-catalyst interface is another important issue in water splitting research. Specifically, the co-catalyst will improve the water spltting performance of Ta_3N_5 especailly at low bias. Co-catalyst has, but limited effect on the onset potential.[13] We have caculated Co_3O_4-Ta_3N_5, $Co(OH)_2$-Ta_3N_5 co-catalysts and GaN-Ta_3N_5 overlayer. The results suggests that the co-catalyst or overlayer will affect the shifts of band edge potentials of Ta_3N_5. The reasons of the band edge shifts resulted from the interface charge transfer. When consideing the effect of termination in Figure S11, we should notice that if different experiental methods affect the morphology and termination of the co-catalyst, the band edge shifts may be different.

References

(1) Bernas, A.; Ferradini, C.; Jay-Gerin, J. P. *Chem. Phys*. **1997**, *222*, 151-160.

(2) Blöchl, P. E. *Phys. Rev. B* **1994**, *50*, 17953-17979.

(3) Perdew, J. P.; Chevary, J. A.; Vosko, S. H.; Jackson, K. A.; Pederson, M. R.; Singh, D. J.; Fiolhais, C. *Phys. Rev. B* **1992**, *46*, 6671-6681.

(4) Perdew, J. P.; Burke, K.; Ernzerhof, M. *Phys. Rev. Lett.* **1996**, *77*, 3865-3868.

(5) Heyd, J.; Scuseria, G. E.; Ernzerhof, M. *J. Chem. Phys*. **2003**, *118*, 8207-8215.

(6) Krukau, A. V.; Vydrov, O. A.; Izmaylov, A. F.; Scuseria, G. E. *J. Chem. Phys*. **2006**, *125*, 224106.

(7) Fan, G.; Wang, X.; Fu, H.; Feng, J.; Li, Z.; Zou, Z. *Phys. Rev. Mater*. **2017**, *1*, 035403.

(8) Brese, N. E.; O'Keeffe, M.; Rauch, P.; DiSalvo, F. J. *Acta. Cryst*. **1991**, *C47*, 2291-2294.

(9) Nosé, S. *J. Chem. Phys*. **1984**, *81*, 511-519.

(10) Hoover, W. G. *Phys. Rev. A* **1985**, *31*, 1695-1697.

(11) Khan, S.; Zapata, M. J. M.; Baptista, D. L.; Goncalves, R. V.; Fernandes, J. A.; Dupont, J.; Santos M. J. L.; Teixeira, S. R. *J. Phys. Chem. C*. **2015**, *119*, 19906–19914.

(12) Wang, J.; Ma, A.; Li, Z.; Jiang, J.; Feng J.; Zou, Z. *Phys. Chem. Chem. Phys.* **2016**, 18, 7938-7945.

(13) Liao, M.; Feng, J.; Luo, W.; Wang, Z.; Zhang, J.; Li, Z.; Yu, T.; Zou, Z. *Adv. Funct. Mater*. **2012**, 22, 3066–3074.